The Astronomical Journal, 129:2585–2596, 2005 June

INTRACLUSTER STARS IN THE VIRGO CLUSTER CORE

J. A. L. Aguerri,[1,2] O. E. Gerhard,[2] M. Arnaboldi,[3] N. R. Napolitano,[4]
N. Castro-Rodriguez,[1] and K. C. Freeman[5]
Received 2004 June 8; accepted 2005 February 19

ABSTRACT

We have investigated the properties of the diffuse light in the Virgo Cluster core region, based on the detection of intracluster planetary nebulae (PNs) in four fields. We eliminate the bias from misclassified faint continuum objects, using improved Monte Carlo simulations, and the contaminations by high-redshift Lyα galaxies, using the Lyα luminosity function in blank fields. Recent spectroscopic observations confirm that our photometric PN samples are well understood. We find that the diffuse stellar population in the Virgo core region is inhomogeneous on scales of 30′–90′: there exist significant field-to-field variations in the number density of PNs and the inferred amount of intracluster light, with some fields empty, some fields dominated by extended Virgo galaxy halos, and some fields dominated by the true intracluster component. There is no clear trend with distance from M87. The mean surface luminosity density, its rms variation, and the mean surface brightness of diffuse light in our four fields are $\Sigma_B = 2.7 \times 10^6\ L_{B\odot}$ arcmin^{-2}, rms $= 2.1 \times 10^6\ L_{B\odot}$ arcmin^{-2}, and $\bar{\mu}_B = 29.0$ mag arcsec^{-2}, respectively. Our results indicate that the Virgo Cluster is a dynamically young environment and that the intracluster component is associated partially with local physical processes like galaxy interactions or harassment. We also argue, based on kinematic evidence, that the so-called over-luminous PNs in the halo of M84 are dynamically associated with this galaxy and must thus be brighter than, and part of a different stellar population from, the normal PN population in elliptical galaxies.

Key words: galaxies: clusters: general — galaxies: clusters: individual (Virgo) — galaxies: evolution — galaxies: interactions — planetary nebulae: general

1. INTRODUCTION

The study of the intracluster light (ICL) began with Zwicky's (1951) claimed discovery of an excess of light between galaxies in the Coma Cluster. Its low surface brightness ($\approx\mu_B > 28$ mag arcsec^{-2}) makes it difficult to study the ICL systematically (Oemler 1973; Thuan & Kormendy 1977; Bernstein et al. 1995; Gregg & West 1998; Gonzalez et al. 2000). A new approach was recently taken by Zibetti et al. (2005), who stacked a large number of SDSS images to reach deep surface brightness levels. In nearby galaxy clusters, intracluster planetary nebulae (ICPNs) can be used as tracers of the ICL; this has the advantages that detection of ICPNs are possible with deep narrowband images and that the ICPN radial velocities can be measured to investigate the dynamics of the ICL component. ICPN candidates have been identified in Virgo (Arnaboldi et al. 1996, 2002, hereafter Paper I, 2003, hereafter Paper II; Feldmeier et al. 1998, 2003, 2004a) and Fornax (Theuns & Warren 1997), with significant numbers of ICPN velocities beginning to become available (Arnaboldi et al. 2004).

The overall amount of the ICL in galaxy clusters is still a matter of debate. However, there is now observational evidence that it may depend on the physical parameters of clusters, with rich galaxy clusters containing 20% or more of their stars in the intracluster component (Gonzalez et al. 2000; Gal-Yam et al. 2003), while the Virgo Cluster has a fraction of ≈10% in the ICL (Ferguson et al. 1998; Durrell et al. 2002; Paper I; Paper II; Feldmeier et al. 2004a), and the fraction of detected intragroup light (IGL) is 1.3% in the M81 group (Feldmeier et al. 2004b) and less than 1.6% in the Leo I group (Castro-Rodríguez et al. 2003). Recent hydrodynamical simulations of galaxy cluster formation in a ΛCDM cosmology have corroborated this observational evidence: in these simulated clusters, the fraction of the ICL increases from ≈10%–20% in clusters with $10^{14}\ M_\odot$ to up to 50% for very massive clusters with $10^{15}\ M_\odot$ (Murante et al. 2004).

The mass fraction and physical properties of the ICL and their dependence on cluster mass will be related with the mechanisms by which the ICL is formed. Theoretical studies predict that if most of the ICL is removed from galaxies because of their interaction with the galaxy cluster potential or in fast encounters with other galaxies, the amount of the ICL should be a function of the galaxy number density (Richstone & Malumuth 1983; Moore et al. 1996). The early theoretical studies about the origin and evolution of the ICL suggested that it might account for between 10% and 70% of the total cluster luminosity (Richstone & Malumuth 1983; Malumuth & Richstone 1984; Miller 1983; Merritt 1983, 1984). These studies were based on analytic estimates of tidal stripping or simulations of individual galaxies orbiting in a smooth gravitational potential. Nowadays, cosmological simulations allow us to study in detail the evolution of galaxies in cluster environments (see, e.g., Moore et al. 1996; Dubinski 1998; Murante et al. 2004; Willman et al. 2004; Sommer-Larsen et al. 2005). Napolitano et al. (2003) investigated the ICL for a Virgo-like cluster in one of these hierarchical simulations, predicting that the ICL in such clusters should be unrelaxed in velocity space and show significant substructures. The first radial velocity measurements for a substantial sample of ICPNs (Arnaboldi et al. 2004) have indeed shown significant field-to-field variations and substructures, and spatial

[1] Instituto de Astrofísica de Canarias, C/Vía Láctea s/n, E-38200 La Laguna, Spain; jalfonso@iac.es, ncastro@iac.es.
[2] Astronomisches Institut der Universitat Basel, Venusstrasse 7, CH-4102 Binningen, Switzerland; ortwin.gerhard@unibas.ch.
[3] Osservatorio Astronomico di Pino Torinese, INAF, I-10025 Pino Torinese, Italy; arnaboldi@to.astro.it.
[4] Kapteyn Astronomical Institute, P. O. Box 800, 9700 AV Groningen, Netherlands; nicola@astro.rug.nl.
[5] Research School of Astronomy and Astrophysics, Mount Stromlo Observatory, Cotter Road, Weston Creek, ACT 2611, Australia; kcf@mso.anu.edu.au.

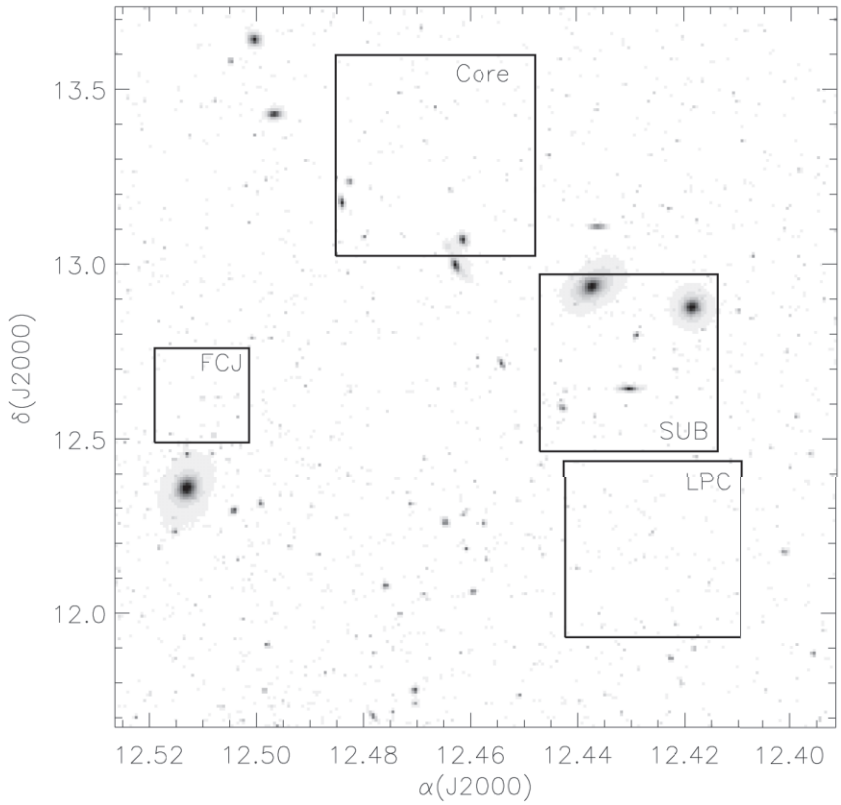

FIG. 1.—Virgo Cluster core region with the positions of the fields studied in this work. The adopted center for the Virgo Cluster is M87.

substructures have been observed in one field in the ICPNs identified with [O III] and Hα (Okamura et al. 2002).

The main goals of this paper are to estimate more reliably the amount of the ICL in the core region of the Virgo Cluster and to investigate the homogeneity of the ICL distribution in this region. Previously, Ferguson et al. (1998) and Durrell et al. (2002) estimated the amount of the ICL by detecting excess red giant stars in two *Hubble Space Telescope* (*HST*) images, while Paper I, Paper II, and Feldmeier et al. (2003, 2004a) obtained deep narrowband images to detect ICPNs in several Virgo fields and then converted to IC luminosity using the bolometric luminosity–specific PN number density for the evolved stellar populations of the M31 bulge (Ciardullo et al. 1989) or for Virgo elliptical galaxies (Jacoby et al. 1990). This gave estimates between 10% and 20% for the fraction of the ICL in different fields. It is not clear at this stage whether this implies a genuine inhomogeneity or whether there are still systematic biases in the different determinations.

Here we study ICPNs in four wide-field images in the Virgo Cluster core. Our observations and data reduction are described in § 2. Then we investigate possible biases in the detection of ICPNs from narrowband surveys and obtain a complete and homogeneous sample of ICPNs in each of the four fields (§ 3). From these data we determine the ICPN luminosity functions (§ 4) and the surface densities of ICPNs and the ICL in these four fields (§ 5). Finally, we discuss the implications of our results in § 6.

2. OBSERVATIONS, DATA REDUCTION, AND SAMPLED FIELDS

We wish to obtain in this work the average observational properties of the diffuse light in the inner region of the Virgo Cluster. (We refer to this region as the core region.) We have selected for this purpose four fields, located within 80′ (≈350 kpc) from the cluster center at M87.[6] Figure 1 shows a Digital Sky Survey (DSS) image of the Virgo Cluster core region, with the positions of the fields studied in this work superposed. The fields were observed with different telescopes and using different instrumentation, as follows.

In 1999 March we observed with the Wide Field Imager on the ESO/MPI 2.2 m telescope a field at α(J2000) = $12^{h}27^{m}48^{s}$ and δ(J2000) = $+13^{\circ}18'46''$; here we refer to this field as the core field. The full image consists of a mosaic of eight 4k × 2k CCD images, covering 34′ × 34′ on the sky. Each CCD has a pixel size of 0.″238, an average readout noise of 4.5 ADU pixel^{-1}, and a gain of 2.2 e^{-} ADU^{-1}. We imaged this field through an 80 Å wide filter centered at 5023 Å, the wavelength of the [O III] λ5007 emission at the Virgo Cluster mean redshift. In addition to this "on-band" filter, we also imaged in the broad *V*-band filter (the "off-band" filter). We took eight individual images of 3000 s for the narrowband filter and eight images of 300 s for the broadband filter. Both broadband and narrowband images were obtained under photometric conditions, and the seeing in the final combined images was 1.″2.

In 2001 February we acquired another field with the Wide Field Camera (WFC) at the 2.5 m Isaac Newton Telescope at the Roque de los Muchachos Observatory (La Palma). The central coordinates of this field are α(J2000) = $12^{h}25^{m}32^{s}$ and δ(J2000) = $+12^{\circ}14'39''$. The WFC detector is made of four CCDs with a total field of view of 34′ × 34′. The pixel scale is 0.″333, and the mean readout noise and gain of the detectors are 6.1 ADU pixel^{-1} and 2.8 e^{-} ADU^{-1}, respectively. We refer to this field hereafter as

[6] Here and in what follows we compute linear scales in Virgo with an adopted distance of 15 Mpc.

TABLE 1
Summary of Field Positions and Filter Characteristics

Field	α (J2000)	δ (J2000)	[O III] Filter λ_c (Å)	[O III] Filter FWHM (Å)	Off-band Filter λ_c (Å)	Off-band Filter FWHM (Å)	C[a]	$m_{\rm lim}(5007)$	$m_{\rm lim}({\rm off})$
Core	12 27 48	+13 18 46	5023	80	5395	894	2.51	27.21	24.75
FCJ	12 30 39	+12 38 10	5027	44	5300	267	2.50	27.01	24.58
LPC	12 25 32	+12 14 39	5027	60	4407	1022	3.02	27.52	25.40
SUB	12 25 47	+12 43 58	5021	74	...	...	2.49	28.10	...
RCN1	12 26 13	+14 08 03	5023	80	5395	894	2.51	26.71	24.75

Note.—Units of right ascension are hours, minutes, and seconds, and units of declination are degrees, arcminutes, and arcseconds.
[a] The term C is the transformation constant between AB and 5007 magnitudes for the narrowband [O III] filters: $m(5007) = m({\rm AB}) + C$.

the La Palma core (LPC) field. The narrowband filter used in these observations was a 60 Å wide filter centered at 5027 Å. The broadband filter was centered on the B band (4407 Å) and was 1022 Å wide. The total exposure time was 27,000 s for the narrowband image and 5400 s for the broadband image. The seeing in the final combined images was 1.″5 in both filters.

We also analyze in the present paper the ICPNs located in one of the fields with photometry from Feldmeier et al. (1998), at $\alpha({\rm J2000}) = 12^{\rm h}30^{\rm m}39^{\rm s}$ and $\delta({\rm J2000}) = +12^\circ38'10''$, and the ICPNs in a field 1° north of the Virgo core with photometry from Arnaboldi et al. (2002) These are subsequently referred to as the FCJ and RCN1 fields, respectively. The RCN1 field is located outside the Virgo core but is very useful for studying the ICPN density profile.

Our sample of fields in the Virgo Cluster core is completed with a field located at $\alpha({\rm J2000}) = 12^{\rm h}25^{\rm m}47^{\rm s}$ and $\delta({\rm J2000}) = +12^\circ43'58''$; we refer to this field as the Subaru core (SUB) field (see Paper II). This field was imaged with the Suprime-Cam 10k × 8k mosaic camera, at the prime focus of the Subaru 8.2 m Telescope. Images were acquired through two narrowband filters, corresponding to [O III] and Hα emission at the redshift of the Virgo Cluster, and two broadband filters, the standard V and R.

The data reduction and calibration of the two new fields presented in this paper (core and LPC) were carried out as for the RCN1 field in Paper I. The data reduction was performed using the MSCRED package in IRAF. For a detailed discussion of the mosaic data reduction, we refer the reader to Alcalá et al. (2002, 2004). Calibrations were obtained using several Landolt fields for the broadband filters and spectrophotometric stars for the narrowband filters. Fluxes were then normalized to the AB magnitude system, following Theuns & Warren (1997). A detailed description of the calibration steps and the relation between AB magnitudes and the "$m(5007)$" [O III] magnitude introduced by Jacoby (1989) are given in Paper I for the FCJ and RCN1 fields and in Paper II for the SUB field. The relations between AB magnitude and $m(5007)$ for the observations of the fields analyzed in the present paper are given in Table 1. In this paper we use the notation of m_n and m_b to refer to the narrowband and broadband magnitudes of the objects in the AB system. We use $m(5007)$ to refer to the [O III] magnitude introduced by Jacoby (1989). Table 1 gives the main observational characteristics of the fields analyzed in this paper.

3. PHOTOMETRY: CATALOG EXTRACTION AND VALIDATION

We used the automatic procedure developed and validated in Paper I for performing the photometry and identification of emission-line objects in our mosaic images in a homogeneous fashion (see Paper I for a full description of the procedure). This procedure was applied to all fields in order to obtain the ICPN photometric candidates. The automatic extraction procedure starts with measuring the photometry of all objects in the images using SExtractor (Bertin & Arnouts 1996). All objects are plotted in a color-magnitude diagram (CMD), $m_n - m_b$ versus m_n, and are classified according to their positions in this diagram. The most reliable ICPN photometric candidates are pointlike sources with no detected continuum emission and observed EW[7] greater than 100 Å, after convolution with the photometric errors as a function of magnitude[8] (see Paper I for more details about the selection criteria). Figure 2 shows the CMD for the core, FCJ, and LPC fields. The final photometric ICPN catalogs, following the selection procedure explained, contain 117, 36, and 14 objects for the core, FCJ, and LPC fields, respectively (see Table 2). The ICPNs in the SUB field were selected from the two-color diagram [O III] − Hα versus [O III] − ($V + R$) calibrated using PNs in M84 (see Paper II for the full description of this method). The number of ICPNs detected in the SUB field was 36, and in RCN1 the number of candidates was 75 (Paper I).

The field-to-field variations observed in the number of ICPN photometric candidates are due in part to the different limiting magnitudes and areas covered by our fields. Limiting magnitudes were obtained following the simulation procedure described in Paper I. We randomly distribute pointlike objects in our final co-added [O III] images, assuming an exponential luminosity function (LF). The photometry of these objects was measured with SExtractor using the same parameters as for the real sources. We define the limiting magnitude for one of our images as the faintest magnitude at which half of the input simulated sample is still retrieved from the image. Table 1 shows the narrowband and off-band limiting magnitudes for all fields. The numbers of ICPN candidates down to the respective [O III] limiting magnitudes are 77, 20, 14, 36, and 55 for the core, FCJ, LPC, SUB, and RCN1 fields, respectively, (see Table 2).

[7] We have computed the observed equivalent width ($\rm EW_{obs}$) using the expression given by Teplitz et al. (2000): $\rm EW_{obs} \approx \Delta\lambda_{nb}(10^{0.4\Delta m} - 1)$, where $\Delta\lambda_{\rm nb}$ is the width of the narrowband filters in angstroms and $\Delta m = m_n - m_b$ is the color of the object, where m_n and m_b are the narrowband and broadband magnitudes, respectively.

[8] The fact that the selection procedure is based on the observed EW greatly reduces the contamination of the ICPN candidate sample by [O II] emitters at $z = 0.35$ whose emission lines would also fall into the narrowband filter bandpasses used for the Virgo photometry. Colless et al. (1990), Hammer et al. (1997), and Hogg et al. (1998) found no [O II] emitters at $z = 0.35$ with observed EW greater than 95 Å.

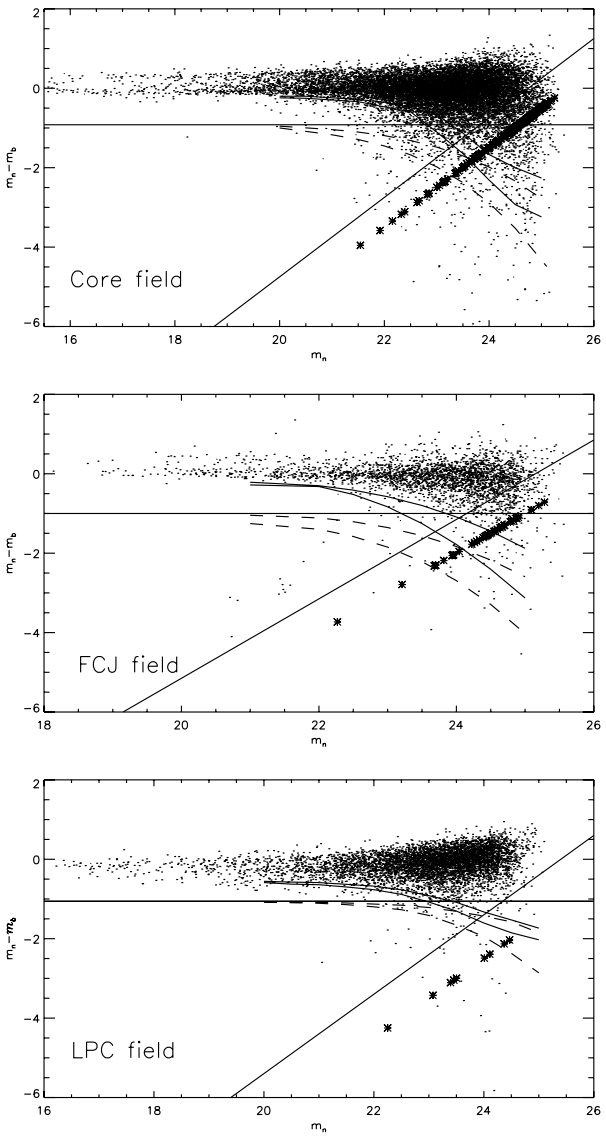

FIG. 2.—CMDs of the core (*top*), FCJ (*middle*), and LPC (*bottom*) fields. The horizontal solid line represents objects with observed EW = 100 Å. The diagonal solid line shows the magnitude corresponding to 1.0 σ above the sky in the off-band images. The solid curved lines represent the 99% and 99.9% lines for the distribution of modeled continuum objects. The dashed curved lines represent the 84% and 97.5% lines for the distribution of modeled objects with observed EW = 110 Å. The points are all objects detected by SExtractor. The asterisks represent those objects with no broadband magnitude measured by SExtractor.

The photometric selection methods can be spectroscopically validated by taking individual spectra of the selected candidates. This is discussed in more detail in § 3.4 below. In the rest of this section we study the possible sources of contaminants for the core, FCJ, LPC, and RCN1 fields, and we statistically subtract the number of contaminants in the photometric samples. This provides more secure ICPN sample sizes, as compared to Paper I.

We do not study the contaminants in the sample of emission-line objects obtained in Paper II for the SUB field. This sample was selected from the detection of emission in two narrow bands ([O III] and Hα). Spectroscopic confirmation was carried out in this field for a subsample of 10 objects at the 3.5 m Telescopio Nazionale Galileo with the DOLORES spectrograph in multiobject spectroscopy (see Paper II). The result was that 8/10 photometrically selected objects were spectroscopically confirmed as emission-line objects. The other two were not detected, probably because of astrometric problems and/or incorrect positioning of the slits (see Paper II).

TABLE 2
NUMBER OF ICPNs IN SURVEYED FIELDS

Field	$N_{\rm ini}$[a]	$N_{\rm mlim}$[b]	$N_{\rm so}$[c]	$N_{\rm lost}$[d]	$N_{\rm Ly\alpha}$[e]	$N_{\rm final}$[f]
Core	117	77	45	1	20/26	13
FCJ	36	20	4	2	2/4	16
LPC	14	14	2	0	22/16	<1
SUB	36	36	...	...	...	36
RCN1	75	55	16	1	3/26	37/15

[a] Total number of objects obtained from the CMDs with our selection criteria as bona fide emission-line objects.
[b] Number of selected emission-line objects down to the [O III] limiting magnitude of each field.
[c] Number of contaminants due to spillover effect.
[d] Number of objects with $EW_{obs} > 110$ Å lost due to photometric errors.
[e] Number of contaminants due to background Lyα galaxies.
[f] Final estimated number of ICPNs.

3.1. *Contamination by Faint Continuum Objects*

It is possible that the ICPN samples in the core, FCJ, LPC, and RCN1 fields may be contaminated by misclassified faint continuum objects, because of the selection based on a threshold in their [O III] fluxes. Because of the photometric errors in their [O III] fluxes, some objects are assigned a flux brighter than their real flux; others are assigned a fainter flux. Because their LF also rises toward faint magnitudes, a significant number of objects will have measured [O III] magnitudes brighter than $m_{\rm lim}$[O III] (or narrowband AB $m_{{\rm lim},n}$), even though in reality they are fainter than the limiting magnitude. In addition, if their fluxes in the off-band image are below the limiting magnitude of that image, these objects will appear in the region of the CMD populated by the selected ICPN candidates, and they will be counted as ICPN candidates even though they are continuum objects (faint stars). We call this "the spillover effect" from faint stars.

Near the $m_{{\rm lim},n}$ limiting magnitude, the number of spillover stars will be negligible if and only if the off-band image is deep enough for detecting the weak continuum flux of these faint objects. This requires that the off-band image has an AB limiting magnitude of at least

$$m_{{\rm lim},b} \simeq m_{{\rm lim},n} + 3\langle {\rm rms} \rangle, \quad (1)$$

where $\langle {\rm rms} \rangle$ is the mean photometric error of objects with magnitude equal to $m_{{\rm lim},n}$. This assumes that the AB color of the stars between off-band and on-band is zero and leaves some margin for the fact that the photometric errors will increase toward fainter magnitudes beyond $m_{{\rm lim},n}$. The $\langle {\rm rms} \rangle$ values for our fields are 0.27, 0.24, 0.19, and 0.23 for the core, FCJ, LPC, and RCN1 fields, respectively. Then, the corresponding off-band images should be 0.81, 0.72, 0.57, and 0.69 mag deeper than the respective on-band images. Table 1 shows the actual limiting magnitudes for the on- and off-band images of our fields. We can see that the off-band image in the core field is only as deep as the core on-band image, suggesting a significant spillover contamination, while the RCN1, FCJ, and LPC fields have off-band images that are deeper than their on-band images by 0.55, 0.6, and 0.9 mag, respectively. In these fields, we can expect that the spillover effect will be less important.

We have performed simulations in order to quantify the spillover effect in the core, FCJ, LPC, and RCN1 fields. First, we

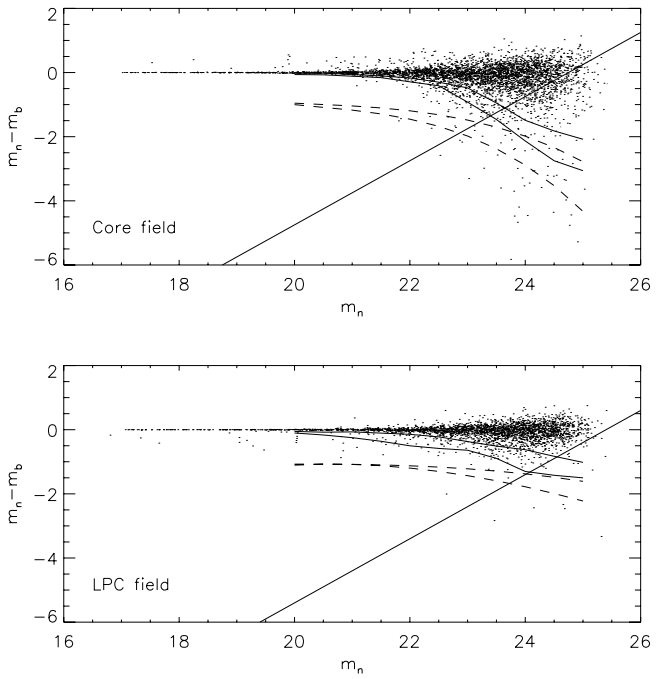

FIG. 3.—CMDs of simulated continuum objects in the core (*top*) and LPC (*bottom*) fields, to quantify the spillover effect from faint stars. The dashed and solid lines are as in Fig. 2.

selected from the photometric catalog of each field as continuum objects those with color $m_n - m_b = [-0.1, 0.1]$. Then we fitted an exponential LF to these objects. For the simulations we randomly distributed on the scientific images several thousand pointlike continuum sources with the same LF as the real continuum objects but extrapolated down to $m_n = 28$. This faint-end magnitude in the simulated continuum sources is $\approx$3 mag fainter than the $m_{\lim,n}$ of the images. The simulated objects were then recovered from the images using the same technique and criteria to measure their photometry as for all sources in the real images. Based on the catalog obtained, we finally constructed the CMD for the recovered simulated objects, as shown in Figure 3. To quantify the spillover effect for each field, we computed the number of simulated objects that are brighter than the corresponding $m_{\lim,n}$ and are located in the region of the ICPN photometric candidates. After scaling the simulations to the same number of observed continuum objects, the final numbers of spillover contaminants brighter than the m_n (or [O III]) limiting magnitude are 45, 4, 2, and 16 for the core, FCJ, LPC, and RCN1 fields, corresponding to 58%, 20%, 14%, and 29% of the ICPN candidates brighter than $m_{\lim,n}$ in these fields, respectively (see also Table 2).

3.2. *Missing ICPNs in the Photometric Samples*

Because of the photometric errors, an emission-line object may have smaller measured EW or fainter m_n magnitude than it would have intrinsically. This means that we can lose in our catalogs some of the emission-line objects with intrinsic $\mathrm{EW_{obs}} > 100$ Å above the magnitude limit. To investigate this possible source of error in our final ICPN photometric samples, we have quantified the number of such objects with simulations. We randomly distributed pointlike objects on the narrowband images following an exponential LF similar to the LF of the PNs in M87 (Ciardullo et al. 1998). No broadband emissions were assigned to these objects. We measured the photometry of them just as for the real sources and studied their distribution in the CMD. We found that 5%, 10%, 1%, and 3% of these objects are lost in our catalogs for the core, FCJ, LPC, and RCN1 fields, respectively (see Table 2). The most important factor that determines these fractions is again the limiting magnitude of the broadband image; in deeper *V*-band images, the smaller rms noise makes it less likely that an object without continuum can be assigned $\mathrm{EW_{obs}} < 100$ Å.

3.3. *Contamination by Background Galaxies*

The photometric samples of ICPNs can also be contaminated by emission-line background galaxies. This is because for [O II] starburst galaxies at $z \simeq 0.35$ and Lyα galaxies at $z \simeq 3.1$ their strong emission lines fall into our narrowband filter width. As pointed out before, the threshold in EW implied by our selection criteria ensures that the selected ICPN photometric samples are nearly free of [O II] contaminants (as also confirmed by the available spectroscopic follow-up observations). However, some Lyα galaxies at $z \simeq 3.1$ can contaminate our ICPN photometric samples. Spectroscopic follow-up observations of ICPNs indeed found that a fraction of the ICPN candidates were Lyα objects (Freeman et al. 2000; Kudritzki et al. 2000; Arnaboldi et al. 2004).

Recently, we imaged an area in the Leo group (Castro-Rodríguez et al. 2003) and extracted emission-line objects using the same selection criteria as for the ICPN photometric candidates in the core, FCJ, LPC, and RCN1 fields. The LF of the emission-line objects selected in the Leo image had a bright cutoff $\approx$1.2 mag fainter than that for the LF of the PNs associated with the elliptical galaxies in the Leo group. The most plausible explanation for this result is that the selected emission-line objects in the image of the Leo group are Lyα background galaxies; two of these were indeed spectroscopically confirmed as Lyα galaxies (see Castro-Rodríguez et al. 2003). This gives us the opportunity to use the Leo image as a blank field to evaluate the contamination of background galaxies in our ICPN photometric catalogs.[9] Taking into account the differences in the surveyed areas and the narrowband filter widths for the Leo and the other fields, we can compute the number of expected Lyα contaminants brighter than the [O III] limiting magnitude in each field, based on the surface density of emission-line sources in the Leo field. The results are 20, 2, 22, and 3 expected Lyα contaminants in the core, FCJ, LPC, and RCN1 fields, respectively (see Table 2).

However, there appear to be intrinsic field-to-field variations in the surface density and LF of Lyα emitters. Figure 4 shows the LF of the emission objects from the Leo field, the spectroscopically confirmed Lyα sample from Kudritzki et al. (2000), and the background sources from the blank field survey of Ciardullo et al. (2002b). It is important to notice that the Leo and Ciardullo et al. (2002b) fields have similar off-band limiting magnitudes. However, the brightest emission objects in the Ciardullo et al. field are 0.6 mag brighter than those in the Leo field and are consistent with the brightest Lyα emitters in the Kudritzki et al. (2000) sample. Using an average Lyα LF obtained from the Ciardullo et al. and Kudritzki et al. samples, we predict the numbers of Lyα contaminants in the core, FCJ, LPC, and RCN1 to be 26, 4, 16, and 26, respectively.

Thus, there is no unique way to estimate the number of high-redshift emission galaxies in our photometric samples, and we have to rely on spectra as much as possible. Fortunately, the predicted number of Lyα contaminants is sensitive to the assumed

[9] We have also simulated the spillover effect in the Leo images. We found that only 6% of the emission-line sample in this field should be due to the spillover from faint stars.

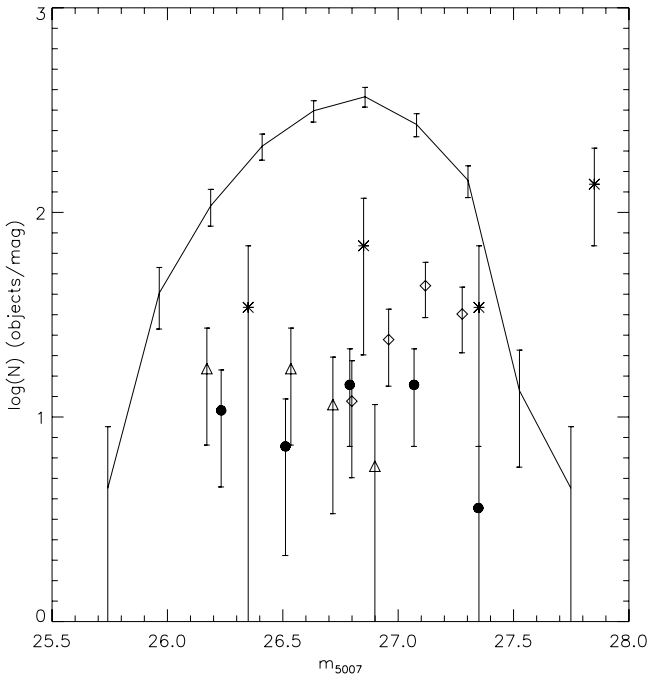

FIG. 4.—ICPN LF in the LPC field (*circles*) compared with the Lyα LF from Kudritzki et al. (2000; *asterisks*), Ciardullo et al. (2002b; *triangles*), and our Leo field (*diamonds*). The LFs of the Lyα emitters were scaled to the effective surveyed volume of the LPC field. The continuous line indicates the PN LF of M87 from the inner 5′ region.

LF only in the RCN1 field. As discussed further in § 3.4, there are very few Lyα emitters in the spectroscopically confirmed emission samples of Arnaboldi et al. (2004) in the core, FCJ, and SUB fields, down to $m(5007) = 27.2$. Based on this result, we use the Leo blank field LF to estimate the Lyα fraction in these fields in Table 2 and what follows.

For the LPC field, Figure 4 shows that the bright cutoff of the emission sources is similar to the bright end of the LF in the samples of Kudritzki et al. (2000) and Ciardullo et al. (2002b), while none of these candidates is as bright as the brightest PNs observed in M87. Furthermore, the number of candidates in the LPC field is small and is in fact smaller than the estimated number of Lyα galaxies expected in this field for either of the two Lyα LFs, down to our magnitude limit. These facts together suggest strongly that all our candidates in this field, including the bright objects, are Lyα emitters. We therefore assume in Table 2 and the subsequent discussion that the number of PNs in the LPC field is <1.

Finally, in the RCN1 field, we have no grounds to prefer one Lyα LF over the other and thus give the number of expected PNs in this field based on both LFs.

3.4. *Comparison with Spectroscopic Results*

Arnaboldi et al. (2004) carried out the spectroscopic follow-up of our selected ICPN samples in the FCJ and core fields and of the ICPN candidates from Okamura et al. (2002) in the SUB field. Spectroscopic observations were done in service mode with the FLAMES spectrograph at UT2 on the VLT, and exposure times were such as to ensure the detection of ICPN candidates with $m(5007) = 27.2$, equivalent to 4.2×10^{-17} ergs cm^{-2} s^{-1} total flux in the line, with a signal-to-noise ratio (S/N) $\simeq 5$.

A total of 70 fibers were allocated to candidates from the above samples with $m(5007) \leq 27.2$; 18/34/18 FLAMES fibers were allocated to sources brighter or equal to 27.2 in the FCJ/core/SUB fields, respectively. Arnaboldi et al. (2004) detected a total of 15/12/13 sharp line emitters and 0/2/0 Lα emitters that show one resolved asymmetric line in these FLAMES pointings. The fraction of confirmed spectra with both components of the [O III] doublet detected was 67%/41%/18%. Given the observing conditions and S/N achieved, these fractions are consistent with the assumption that all of the sharp line emitters are indeed PNs. Thus, for [O III] fluxes such that $m(5007) \leq 27.2$, the contamination by background galaxies is small.

The remaining spectra in the Arnaboldi et al. (2004) observations did non show any spectral features in the wavelength range covered by FLAMES. As we have seen in §§ 3.1–3.3, one should indeed expect a fraction of candidates in the candidate samples to be contaminants because of the spillover effect, i.e., faint continuum stars erroneously classified as ICPNs because of a shallow off-band image. Thus, the predicted spectroscopic confirmation rates, given as the fraction of true ICPNs in these candidate samples, varied strongly from field to field, despite similar $m_{\rm lim}(5007)$. The spectroscopic follow-up, as well as earlier spectroscopic observations by Kudritzki et al. (2000) and the comparison with deeper narrowband imaging in [O III] and Hα (Paper II), provide direct evidence for contamination by faint stars in narrowband [O III] ICPN surveys. Contamination from faint stars is also a possible explanation for the somewhat low spectroscopic confirmation rate for the PN samples in elliptical galaxies (Arnaboldi et al. 1996, 1998).

Arnaboldi et al. (2004) compared the expected spectroscopic confirmation rates based on the simulations in the present paper with those determined with FLAMES. They are in close agreement, showing that the photometric samples are now well understood. A high confirmation rate (small contamination) can be achieved when the off-band image is sufficiently deep.

4. ICPN LUMINOSITY FUNCTION

4.1. *The Necessity of Deep Off-Band Images*

Figure 5 shows the LFs of the ICPN photometric candidates (*circles*) in all fields but LPC. We have also superposed the LFs of misclassified stars (*asterisks*). A comparison with Figure 4 shows that the LF of the Lyα galaxies has a fainter cutoff than the LF of the photometric ICPN candidates in these fields. Thus, the brightest bins of the ICPN LF are free of Lyα contaminants. There exist brighter Lyα galaxies, but these often have a measurable continuum (Kudritzki et al. 2000). The brightest LF bins are also free of misclassified stars in most fields; however, in the core field the ICPN LF is affected by misclassified stars at all magnitudes. This demonstrates again the importance of obtaining deep broadband images. Figure 5 also contains the LF of the ICPN candidates from the SUB field, which is free of contaminants in all bins.

We have fitted the standard PN LF to the three brightest magnitude bins (not affected by contaminants) of the ICPN LF in the FCJ and RCN1 fields. The six brightest bins were considered in the fit of the ICPN LF in the SUB field. In both cases, the LF was first convolved with the photometric errors. The fitted empirical exponential LF is given by

$$N(m) = c_1 e^{c_2 M}[1 - e^{3(M^* - M)}], \qquad (2)$$

where c_1 is a positive normalization constant to be determined, $c_2 = 0.307$, and we adopt a cutoff $M^*(5007) = -4.51$ (Ciardullo et al. 1989, 2002a). The resulting apparent magnitudes of the bright cutoffs (m^*) obtained from the fits are 25.9 ± 0.2, 26.0 ± 0.3, and 26.3 ± 0.15 for the RCN1, FCJ, and SUB samples,

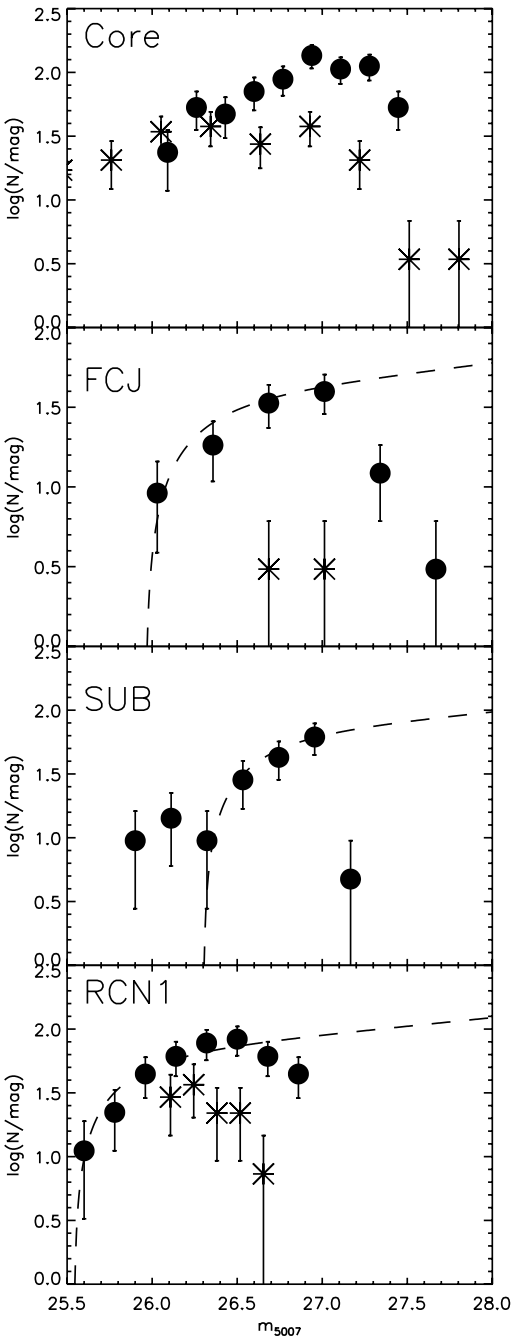

FIG. 5.—LFs of all ICPN photometric candidates (*circles*) in the core, FCJ, SUB, and RCN1 fields. The asterisks represent the LFs of the simulated spillover stars. The dashed lines represent the fitted LFs.

respectively. For reference, we report here the m^* value fitted to the PN LF from the inner region of M87, which amounts to 26.37.

4.2. *The Nature of Overluminous PNs and the Bright Cutoff of the LF*

The bright cutoff of the PN LF has been extensively used as a distance indicator in extragalactic astronomy (Ciardullo et al. 2002a). An implicit assumption of the PN LF method is that all the PNs that make up the observed LF are at the same distance. In a Virgo-like cluster, its finite depth can distort the PN LF, since the ICPNs at shorter distances can contribute to the observed LF and produce a brighter cutoff, as discussed in Ciardullo et al. (1998), Paper I, and Feldmeier et al. (2004a).

However, the bright cutoff can also be affected by the age (Marigo et al. 2004) or metallicity (Dopita et al. 1992) of the stellar population; e.g., the dependence of M^* with metallicity, $\Delta M^* = 0.928[\mathrm{O/H}]^2 + 0.225[\mathrm{O/H}] + 0.014$ (Dopita et al. 1992; Ciardullo et al. 2002a), can produce a change of the cutoff magnitude of a similar order to the reported line-of-sight (LOS) distortions. The analysis of our ICPN LFs combined with the spectroscopic results of Arnaboldi et al. (2004) can clarify the relative importance of these effects.

The bright cutoff of our ICPN LF in the FCJ field is 0.37 mag brighter than the bright cutoff of the PN LF of M87 (Ciardullo et al. 1998). In Paper I we considered that this (substantial) difference would most plausibly be explained if the ICPNs in the FCJ field are located in front of M87. Assuming a distance of 15 Mpc for M87, the brightest of the ICPNs in the FCJ field would be located 2.3 ± 1.5 Mpc in front of M87, indicating a substantial LOS depth of the Virgo Cluster, consistent with other measurements.

The spectroscopic follow-up in FCJ has shown a velocity distribution that is dominated by a narrow peak related to the halo of M87 (Arnaboldi et al. 2004). In addition to this peak, there are three kinematic outliers, which are all also unusually bright, with fluxes in the bright falloff of the M87 PN LF, so that they shift the FCJ LF to a brighter cutoff. The correlation between their discrepant radial velocities and bright $m(5007)$ support the hypothesis that these are ICPNs free-flying in Virgo intracluster space and not gravitationally bound to M87. LOS effects are therefore a viable explanation for the brighter cutoff in this field.

No spectroscopic follow-up is yet available for the RCN1 sample, but the absence of bright galaxies and a very similar PN LF to that in FCJ suggest that LOS effects may also be the most likely explanation for the bright cutoff in this field, as already discussed in Paper I.

The PN LF for the ICPN sample in the SUB field differs from those of RCN1 and FCJ: five ICPNs appear to be up to 0.3 mag brighter than the remaining smoother, more regular distribution, similar to those measured for ICPNs in FCJ and RCN1 (see Fig. 5). Can the overluminous ICPNs in SUB be on the near side of the cluster? The spectroscopic follow-up of Arnaboldi et al. (2004) contained three of these objects and confirmed them as PNs. However, their radial velocities are consistent with the dynamics of M84. The kinematic observations make it unlikely that these objects are 2 Mpc in front of M84; most likely they are at the same position as M84 within the Virgo Cluster, and LOS effects are unimportant. Furthermore, the PN LF fit to only the remaining, smoother distribution gives a distance modulus of 30.95 ± 0.15; from the LF of PNs associated directly with M84, the distance modulus of M84 is 30.98 (Jacoby et al. 1990). Thus, within the errors, M84 and the bulk of the IC stellar population in the SUB field are at the same distance.

The other alternative for the overluminous PNs in SUB is that they came from a different stellar population, which could be either younger than or of different metallicity than the main M84 stellar population (see Marigo et al. 2004). Perhaps they are associated with the infall of some dwarf galaxies into M84. Furthermore, the PNs in this field show a nonuniform spatial distribution. Most of them are located in a loop near M84 (see Okamura et al. 2002). This also supports the scenario that they are associated with some harassment or infall process involving M84.

4.3. *The Relative Distances of M87 and M84*

Neilsen & Tsvetanov (2000) and West & Blakeslee (2000) have used surface brightness fluctuation (SBF) distances to consider

the three-dimensional structure of the Virgo Cluster elliptical galaxies and found that most of these are arranged in a nearly colinear structure extending ±(2–3) Mpc from M87. The M84/M86 subgroup is falling into the Virgo Cluster from behind and is itself on the far side of the main Virgo Cluster.

We have tested the relative distance of these subunits in Virgo based on the most recent PN data sets obtained for these galaxies, the Ciardullo et al. (1998) sample for M87 and the Paper II data for M84. We have run a Kolmogorov-Smirnov (K-S) test of the PN LFs associated with M84 and the inner 5′ region of M87, without the overluminous PNs. The K-S test cannot exclude that the two LFs came from the same distribution function. Thus, the PN LF method based on recent PN data sets places M84 and M87 at similar distances.

5. SURFACE DENSITY AND FRACTION OF ICL IN DIFFERENT FIELDS

5.1. *ICPNs in the Different Fields*

The observations of the different Virgo fields that we have used in this study have slightly different filters, survey areas, and [O III] limiting magnitudes. Depending on the cluster dynamics, the filter bandpass may cut out a few ICPNs; the most likely field for this is the FCJ field.[10] Before we compare the number density of ICPNs in these fields and derive the average amount of ICL in the Virgo Cluster core, we should establish a sample of ICPNs with the same flux limit. To this end we multiply the number of ICPNs for each field by the factor

$$\Delta \equiv \frac{\int_{M^*}^{M^*+1} N(m)\,dm}{\int_{m^*}^{m_{\rm lim}} N(m)\,dm}, \qquad (3)$$

where $N(m)$ is given by equation (2), M^* and m^* denote the absolute and apparent magnitude of its bright cutoff, respectively, and $m_{\rm lim}$ is the [O III] limiting magnitude in each field. In scaling the various field samples by this factor, we obtain the respective number of ICPNs down to a limiting absolute magnitude $M^* + 1$. The number of emission-line candidates in the LPC field was not scaled, because we saw in § 3.3 that they are all compatible with being Lyα background galaxies. For this field we give an upper limit for the amount of the ICL, assuming that the number of ICPNs in the field is <1. For the core field, we could not fit the ICPN LF, because it is contaminated by spillover objects for all magnitudes. Thus, to compute Δ for this field we have used the PN LF of M87 (Ciardullo et al. 1998). We have also checked that both spillover and Lyα contaminants do not affect the brightest bins of the ICPN LF of RCN1, so that the LF fitted in Paper I is still valid. We used this LF in order to scale the number of ICPNs in the RCN1 field down to $M^* + 1$. The scaling factors, final numbers, and resulting surface densities of ICPNs for the different fields are given in Table 3.

TABLE 3
NUMBER OF ICPNS WITHIN $M^* + 1$ IN SURVEYED FIELDS

Field	$N_{\rm mlim}$[a]	Δ[b]	$N_{\rm ICPNs}$[c]	Area (arcmin^2)	ICPNs arcmin^{-2}
Core	13	1.28	17	943	0.018
FCJ	16	0.98	15	266	0.056
LPC	1	...	1	744	0.001
SUB	36	0.40	14	706	0.020
RCN1	37/15	1.15	43/17	957	0.045/0.018

[a] Number of estimated emission-line objects brighter than the [O III] limiting magnitude in each field.
[b] Scale factor.
[c] Final number of ICPNs.

5.2. *From the ICPN Surface Density to Surface Brightness of the ICL: The α Parameter*

In principle, determining the amount of the ICL from the observed numbers of ICPNs is straightforward. From Méndez et al. (1993), if $\dot{\epsilon}$ is the specific PN formation rate in PNs yr^{-1} $L_\odot^{-1}$, L_T is the total bolometric luminosity of a sampled population, and $t_{\rm PN}$ is the lifetime of a PN, which we take as 25,000 yr, then the corresponding number of PNs, $n_{\rm PN}$, is

$$n_{\rm PN} = \dot{\epsilon} L_T t_{\rm PN}. \qquad (4)$$

Theories of stellar evolution predict that the specific PN formation rate should be $\sim 2 \times 10^{-11}$ stars yr^{-1} $L_\odot^{-1}$, nearly independent of population age or initial mass function (IMF) (Renzini & Buzzoni 1986). Every stellar system should then have $n_{\rm PN} = \alpha L_T = 50 \times 10^{-8}$ PNs $L_\odot^{-1} \times L_T$. If the PN LF of equation (2) is valid 8 mag down from the cutoff, one can determine the fraction of PNs within 2.5 mag of the cutoff and thus define $\alpha_{2.5}$ as the number of PNs within 2.5 mag of M^* associated with a stellar population of total luminosity L_T. Approximately one out of 10 of these PNs are within 2.5 mag of M^*, and following from the above assumptions, most stellar populations should have $\alpha_{2.5} \sim 50 \times 10^{-9}$ PNs $L_\odot^{-1}$ (Feldmeier et al. 2004a). The observed number of ICPNs can then be used to infer the total luminosity of the parent stellar population.

However, as first noticed by Peimbert (1990), observations of PN samples in galaxies show that $\alpha_{2.5}$ varies strongly as a function of color. Hui et al. (1993) found that $\alpha_{2.5}$ decreases by a factor of 7 from the value of $\approx 50 \times 10^{-9}$ PN $L_\odot^{-1}$ measured in dwarf elliptical galaxies like NGC 205 (Burstein et al. 1987) to $\approx 7 \times 10^{-9}$ PN $L_\odot^{-1}$ observed in Virgo giant elliptical galaxies (Jacoby et al. 1990).

The amount of the ICL depends directly on the adopted value of α, which is thus not very well constrained and is a function of the $(B - V)$ color of the parent stellar population, currently unknown for the Virgo ICL. To take this uncertainty into account in our estimates of the intracluster luminosity in the different fields, we consider three plausible values for α, which are (1) the value appropriate for an evolved population like that of the M31 bulge (Ciardullo et al. 1989), (2) the value determined by Durrell et al. (2002) for the intracluster red giant branch (RGB) stars observed with *HST*; and (3) the value determined from the Hui et al. (1993) empirical relation. In this case the $(B - V)$ of the parent stellar population is determined from the average colors of the Virgo galaxies near the field position.

The scaling adopted in our work ensures that we have taken into account all bona fide ICPNs within 1 mag of M^*. We then use the corresponding value $\alpha_{1.0}$ to infer the amount of IC luminosity in our fields; from equation (2), $\alpha_{1.0}/\alpha_{2.5} \approx 0.24$. Furthermore, we adopt the conversion from bolometric to B-band luminosity as in Ciardullo et al. (1989). Table 4 gives the resulting values for the B-band luminosity and surface brightness in our fields, in each case for the three values of α (1–3). The interval given by the lowest and the largest value of the luminosity (surface brightness) thus determined from the number of

[10] For the mean redshift of the Virgo Cluster and a velocity dispersion $\sigma_{\rm cluster} = 800$ km s^{-1}, the width of the FCJ on-band filter covers the velocities in the $-1.5\sigma_{\rm cluster}$ to $+1.8\sigma_{\rm cluster}$ range.

TABLE 4
SURFACE BRIGHTNESS OF THE ICL IN THE SURVEYED FIELDS

Field	$\alpha_{1.0,B}$ (10^{-9})	$L_{\rm ICL}$ arcmin^{-2} ($10^6\ L_{\odot,B}$ arcmin^{-2})	μ_B (mag arcsec^{-2})	% Local[a]
Core	9.40	1.91	29.5	10
	13.30	1.35	29.8	7
	10.59	1.70	29.6	9
FCJ	9.40	5.96	28.2	8
	13.30	4.21	28.6	6
	7.46	7.51	28.0	10
LPC	9.40	0.11	32.6	0.5
	13.30	0.08	32.9	0.3
	25.44	0.04	33.7	0.2
SUB	9.40	2.13	29.4	2
	13.30	1.50	29.7	1
	3.46	5.78	28.3	5
RCN1	9.40	4.79/1.91	28.5/29.5	51/29
	13.30	3.38/1.35	28.9/29.9	42/23
	15.00	3.00/1.20	29.0/30.0	39/21

[a] Contribution of the ICL to the total light in galaxies at the local position of the field.

ICPNs in each field is our *best estimated range* for the IC luminosity (surface brightness) in that field.

5.3. *Field-to-Field Variation and the Dependence with Distance from the Cluster Center*

We consider first the field-to-field variations in the number of ICPN candidates as reported in Table 3. Figure 6 shows the ICPN number densities in our fields with their Poisson errors. The overdensity observed at the FCJ field position is significant at the 2–3 σ level with respect to the number densities observed in core and SUB. The low density of ICPNs in the LPC field is significant at the $\sim$4 σ level with respect to the number densities observed in FCJ, core, and SUB. The low upper limit to the number of ICPNs in LPC confirms earlier findings by Kudritzki et al. (2000) for an adjacent field, centered at α(J2000) = $12^{\rm h}26^{\rm m}32\overset{\rm s}{.}1$, δ(J2000) = $+12^\circ14'39''$.

The number density plot also shows no clear trend with distance from the cluster center at M87, except that the value in the innermost FCJ field is high. However, the spectroscopic results of Arnaboldi et al. (2004) have shown that 12/15 PNs in this field have a low velocity dispersion of 250 km s^{-1}, i.e., in fact belong to the outer halo of M87, which thus extends to at least 65 kpc radius. In the SUB field, 8/13 PNs belong to the similarly cold, extended halo of M84, while the remaining PNs are observed at velocities that are close to the systemic velocities of M86 and NGC 4388, the two other large galaxies in or near this field. It is possible that in a cluster as young and unrelaxed as Virgo, a substantial fraction of the ICL is still bound to the extended halos of galaxies, whereas in denser and older clusters these halos might already have been stripped. If so, it is not inappropriate to already count the luminosity in these halos as part of the ICL. However, in Figure 6 we also give the plot of the PN number density with radius for the case in which the PNs in the outer halos of M87 and M84 are removed from the FCJ and SUB samples. In this case, the resulting number density is even more nearly flat with radius, but there are still significant field-to-field variations; in particular, the remaining number densities in SUB and LPC are low.

We next consider the luminosity densities and surface brightnesses of the ICL in our fields and their dependence on the distance from the cluster center. This introduces the additional uncertainty of the α parameter; when the range of α from § 5.2

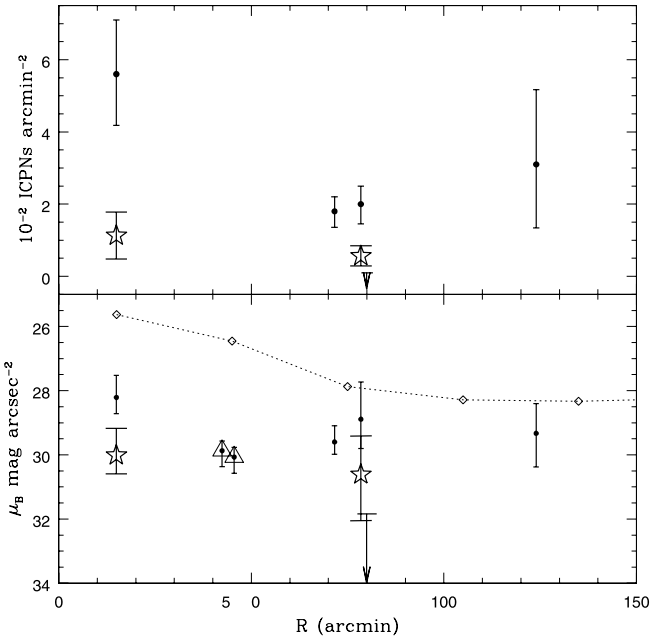

FIG. 6.—Number density of PNs (*top*) and surface brightness (*bottom*) in our surveyed fields. In the top panel, circles show the measured number densities from Table 3, and error bars denote the Poisson errors. For the LPC field our upper limit is given. For the RCN1 field at the largest distance from M87, the uncertainty from the correction for Lyα emitters is substantial and is included in the error bar. The large stars with Poisson error bars show the number densities of PNs in FCJ and SUB fields not including PNs bound to the halos of M87 and M84. In the lower panel, circles show the surface brightness inferred with the average value of α in Table 4, and error bars show the range of values implied by the Poisson errors and the range of adopted α values. Triangles represent the measurements of the ICL from RGB stars; error bars indicate uncertainties in the metallicity, age, and distance of the parent population as discussed in Durrell et al. (2002). The stars indicate the surface brightness associated with the ICPNs in the FCJ and SUB fields that are not associated with the M87 or M84 halos but are free flying in the Virgo Cluster potential, (Arnaboldi et al. 2004). The dashed line and diamonds show the *B*-band luminosity of Virgo galaxies averaged in rings (Binggeli et al. 1987). Distances are relative to M87. The ICL shows no trend with cluster radius out to 150′.

is taken into account, the total uncertainties in the luminosity density increase, and differences between the various fields become less significant. Data are given in Table 4. The bottom panel of Figure 6 shows the radial variation of the surface brightness as a function of distance from M87. In the FCJ and SUB fields, we again show two points, one derived from all PNs and one based on only the PNs that are not kinematically associated with the M87 or M84 halo. Again, there is thus no clear radial trend with distance: the ICL surface brightness in Virgo is consistent with a constant value, with the exception of the low value in the LPC field. As representative values for the surface luminosity density and the surface brightness in the Virgo core region, we take the average for our four fields, including the M87 and M84 halo PNs, and use for each field the respective average value of α in Table 4: $\Sigma_B = 2.7 \times 10^6\ L_{B\odot}$ arcmin^{-2}, and $\bar{\mu}_B = 29.0$ mag arcsec^{-2}. Note, however, the large rms $= 2.1 \times 10^6\ L_{B\odot}$ arcmin^{-2}, due to the field-to-field variations and the adopted range in α.

Ferguson et al. (1998) and Durrell et al. (2002) measured the ICL in two *HST* fields near M87 by counting excess intracluster RGB stars. One can estimate the surface brightness of the underlying stellar population, given assumptions on the metallicity, age, IMF, and average distance for this stellar population. From the total flux associated with the 630 excess sources detected in their *HST* field, Ferguson et al. (1998) computed that the surface brightness and surface luminosity density of the ICL in their field 45.′8 northeast of M87 are 31.11 mag arcsec^{-2} and $0.42 \times 10^6\ L_{B\odot}$ arcmin^{-2}, respectively. Durrell et al. (2002) used the same technique in a field 42.′3 northwest of M87 and detected $\sim$50% greater number of stars than Ferguson et al. (1998). From their best-fit models to the LF, Durrell et al. obtain $\mu_B = 30.07$ and 29.677 mag arcsec^{-2} for the northeast and northwest *HST* fields, respectively. We have superposed these values in Figure 6. It can be seen that they are in good agreement with our inferred surface brightness, and still no clear radial trend is evident. Averaging our results and the RGB data, the mean surface luminosity density and surface brightness of the ICL in the combined fields in the Virgo core region (the RCN1 field not included) become $2.2 \times 10^6\ L_{B\odot}$ arcmin^{-2} and 29.3 mag arcsec^{-2}, respectively.

5.4. *Luminosity Fraction of the ICL in the Virgo Core*

Surface luminosity densities associated with both ICPNs and RGB stars depend in large part on the assumed metallicity, age, and IMF for the parent stellar population in the LOS. The fact that our best estimates are given as intervals in luminosities reflects a limitation in our knowledge of the stellar populations and of post-AGB stellar evolution, rather than uncertainties in the ICPN numbers from photometric catalogs, which are now well understood.

When we compare the luminosity of the ICL at the positions of our fields with the luminosity from the Virgo galaxies, we add in further uncertainties, because the luminosities of nearby Virgo galaxies depend very much on the location and field size surveyed in the Virgo Cluster. We therefore consider the reported intervals in surface brightness to be our primary result, while the relative fractions of the ICL with respect to the Virgo galaxy light are evaluated for comparison with previous ICPN works only, and we consider them to be more uncertain.

Our approach is to assume that the ICL is related to local galaxies in each field, based on the spectroscopic results of Arnaboldi et al. (2004) that show the Virgo Cluster to be very inhomogeneous and still dynamically young. We thus compare the luminosity of the ICL with that from the Virgo galaxies located in the field. We have obtained from the DSS archive the images centered on our fields with a radius of 120′ and convolved each image with a Gaussian with σ equal to the radius of our corresponding images. Then, we determined the total luminosity in an area equal to the surveyed area of each field. We thus obtained 1.67×10^{10}, 1.40×10^{10}, 1.76×10^{10}, and $4.41 \times 10^9\ L_{B\odot}$ for the core, FCJ, LPC, and RCN1 fields, respectively. The galaxy light in the SUB field is dominated by the three bright galaxies in this field, M86, M84, and NGC 4388. Their combined luminosity is $7.2 \times 10^{10}\ L_{B\odot}$ (see Paper II). The contribution of the ICL to the total light in each field based on this local comparison is given in Table 4; the mean fraction for our four fields in the Virgo core is 5%. However, there are significant field-to-field variations. The fraction of the ICL versus total light ranges from $\simeq$8% in the core and FCJ fields, to less than 1% in the LPC field, which in its low ICL fraction is similar to low-density environments (Castro-Rodríguez et al. 2003).

5.5. *Discussion*

The data presented here constitute a sizable sample of ICPNs in the Virgo core region, constructed homogeneously and according to rigorous selection criteria. From the study of four wide fields in the Virgo core we obtain a mean surface luminosity density of $2.7 \times 10^6\ L_{B\odot}$ arcmin^{-2}, rms $= 2.1 \times 10^6\ L_{B\odot}$ arcmin^{-2}, and a mean surface brightness of $\mu_B = 29.0$ mag arcsec^{-2}. Often these numbers are translated into fractions of the ICL with respect to light in galaxies at the cluster positions, and our best estimate in the Virgo core is $\sim$5%.

We can compare the amount of the ICL in the Virgo Cluster core region with that measured in the RCN1 field (see Paper I). The surface luminosity density and surface brightness intervals evaluated for this field are similar to those for the FCJ. The RCN1 field contains no bright galaxies, however, so these values translate into a significantly higher fraction of the ICL with respect to Virgo galaxy light, $\simeq$34%. If we include the RCN1 measurements in our average, the mean surface luminosity becomes $2.7 \times 10^6\ L_{B\odot}$ arcmin^{-2}, rms $= 1.9 \times 10^6\ L_{B\odot}$ arcmin^{-2}, and the mean surface brightness $\mu_B = 29.1$ mag arcsec^{-2}. The average fraction of the ICL with respect to Virgo Cluster galaxy light then becomes $\sim$10%.

Previous works on the ICL using ICPN tracers have claimed larger average fractions for the ICL in the Virgo core (15.8%, Feldmeier et al. 2004a; 15%, Durrell et al. 2002), despite similar inferred surface brightnesses for the ICL as shown in Figure 6. These higher fractions reflect only a difference in the normalization relative to the Virgo galaxy light. Furthermore, the Feldmeier et al. (2004a) fields in the Virgo subcluster A are closer on average to M87 ($\sim$25′) than our fields; thus, they may be more dominated by the M87 halo, as indicated by the spectroscopic follow-up of the ICPN sample in the FCJ field (Arnaboldi et al. 2004). These radial velocity measurements indicate the presence of a stellar population at equilibrium in the M87 halo, and only $3/15 = 1/5$ of all PN candidates in the FCJ field are therefore "truly" intracluster. The spectroscopic follow-up of Arnaboldi et al. (2004) has confirmed the expected fraction of ICPN candidates in the other fields, therefore supporting our determinations from the PN observations.

The field-to-field variations in the measured number density of ICPNs and the high value in the outer RCN1 field indicate that the ICL is still not relaxed in the cluster potential. There has not been enough time for phase mixing to erase these variations. This places a strong constraint on the age and origin of the ICL in the Virgo Cluster core region, which must have been brought

into this location not much more than a few dynamical times ago, where (Binney & Tremaine 1987)

$$t_{\rm dyn} = \sqrt{\frac{3\pi}{16G\rho}}, \quad (5)$$

and ρ is the mean density enclosed within the field distance from the center of the cluster. We have computed $t_{\rm dyn}$ using the mass distribution given by Nulsen & Bohringer (1995) for the central regions of the Virgo Cluster. The dynamical times at the locations of our fields are from $\sim 2 \times 10^8$ yr for the FCJ field to $\sim 8 \times 10^8$ yr for the LPC and SUB fields. The FCJ field has the shorter dynamical time because it is located close to M87 ($\approx$65 kpc). From these estimated dynamical times, phase mixing to erase the field-to-field variations in the ICL light would take a few gigayears. The observed field-to-field variations thus suggest that the Virgo Cluster is dynamically young, confirming the similar inference from the inhomogeneous radial velocity distributions by Arnaboldi et al. (2004).

Recent cosmological simulations have measured the amount of diffuse light in simulated galaxy clusters (Murante et al. 2004; Sommer-Larsen et al. 2005). They conclude that the mass of the diffuse light varies with the mass of the cluster, being larger for more massive clusters. Murante et al. (2004) studied the diffuse light for clusters with masses in the range 10^{14}–$10^{15}\ M_\odot$. They found for low-mass clusters like Virgo ($\approx 10^{14}\ M_\odot$) that the surface mass density of the diffuse light in the innermost regions of the clusters is $\approx 10^7\ h\ M_\odot\ {\rm kpc}^{-2}$, which is in agreement with our measured mean surface luminosity density of the ICL in the Virgo core of $2.7 \times 10^6\ L_{B\odot}\ {\rm arcmin}^{-2}$, for a mass-to-light ratio of $\sim$5, as expected for an evolved stellar population.

6. CONCLUSIONS

Four pointings around the core region of the Virgo Cluster have been analyzed to determine the amount of the intracluster light (ICL) via intracluster planetary nebulae (ICPNs). The photometric ICPN candidates for three of the fields were selected according to the on-off band technique using [O III] λ5007, and for the fourth field by the emission in [O III] and Hα. We have carefully studied the contribution of different contaminants to the photometric samples of ICPNs using simulations on our images. In this way we obtain a well-understood, magnitude-limited sample of ICPN candidates.

In the SUB field, spectroscopic follow-up has provided kinematic evidence that the so-called overluminous PNs in the halo of M84 are dynamically associated with this galaxy. They must therefore be intrinsically brighter than the normal elliptical galaxy PN population in M84, presumably due to a younger age or different metallicity.

Based on our new sample of ICPNs, the mean surface brightness and surface luminosity density of the ICL in our four fields are $\mu_B = 29.0$ mag arcsec^{-2} and $2.7 \times 10^6\ L_{B\odot}$ arcmin^{-2}, respectively. These values are in good agreement with the corresponding values obtained from excess red giant counts in two *HST* images in the Virgo core. There is no trend evident with distance from M87. When the fraction of the ICL is computed for our four fields in the Virgo core, it amounts to 5% of the total galaxy light.

However, the diffuse stellar population in Virgo is inhomogeneous on scales of 30′–90′: we observe substantial field-to-field variations in the number density of PNs and the inferred amount of ICL, with some fields empty, some fields dominated by extended Virgo galaxy halos, and some fields dominated by the true intracluster component.

The field-to-field variations indicate that the ICL is not yet dynamically mixed. This imposes a constraint on the time of origin of the ICL and the Virgo Cluster itself. The lack of phase mixing suggests that both have formed in the last few gigayears and that local processes like galaxy interactions and harassment have played an important role in this. In a cluster as young and unrelaxed as Virgo, a substantial fraction of the ICL may still be bound to the extended halos of galaxies, whereas in denser and older clusters these halos might already have been stripped.

We wish to thank an anonymous referee for insightful comments. We thank ESO, Subaru, and the Isaac Newton Group of Telescopes for the observing time allocated to this project. We acknowledge financial support by SNF grants 20-56888.99 and 200020-101766 and by INAF projects of national interests (PI: M. A.) J. A. L. A. acknowledges funding by the Spanish DGES, grant AYA2001-3939; N. R. N. was supported by a Marie Curie fellowship.

REFERENCES

Alcalá, J. M., et al. 2002, Proc. SPIE, 4836, 406
———. 2004, A&A, 428, 339
Arnaboldi, M., et al. 1996, ApJ, 472, 145
———. 1998, ApJ, 507, 759
———. 2002, AJ, 123, 760 (Paper I)
———. 2003, AJ, 125, 514 (Paper II)
———. 2004, ApJ, 614, L33
Bernstein, G. M., Nichol, R. C., Tyson, J. A., Ulmer, M. P., & Wittman, D. 1995, AJ, 110, 1507
Bertin, E., & Arnouts, S. 1996, A&AS, 117, 393
Binggeli, B., Tammann, G. A., & Sandage, A. 1987, AJ, 94, 251
Binney, J. J., & Tremaine, S. 1987, Galactic Dynamics (Princeton: Princeton Univ. Press)
Burstein, D., Davies, R. L., Dressler, A., Faber, S. M., Stone, R. P. S., Lynden-Bell, D., Terlevich, R. J., & Wegner, G. 1987, ApJS, 64, 601
Castro-Rodríguez, N., Aguerri, J. A. L., Arnaboldi, M., Gerhard, O., Freeman, K. C., Napolitano, N. R., & Capaccioli, M. 2003, A&A, 405, 803
Ciardullo, R., Feldmeier, J. J., Jacoby, G. H., Kuzio de Naray, R., Laychak, M. B., & Durrell, P. R. 2002a, ApJ, 577, 31
Ciardullo, R., Feldmeier, J. J., Krelove, K., Jacoby, G. H., & Gronwall, C. 2002b, ApJ, 566, 784
Ciardullo, R., Jacoby, G. H., Feldmeier, J. J., & Bartlett, R. E. 1998, ApJ, 492, 62
Ciardullo, R., Jacoby, G. H., Ford, H. C., & Neill, J. D. 1989, ApJ, 339, 53
Colless, M., Ellis, R. S., Taylor, K., & Hook, R. N. 1990, MNRAS, 244, 408
Dopita, M. A., Jacoby, G. H., & Vassiliadis, E. 1992, ApJ, 389, 27
Dubinski, J. 1998, ApJ, 502, 141
Durrell, P. R., Ciardullo, R., Feldmeier, J. J., Jacoby, G. H., & Sigurdsson, S. 2002, ApJ, 570, 119
Feldmeier, J. J., Ciardullo, R., & Jacoby, G. H. 1998, ApJ, 503, 109
Feldmeier, J. J., Ciardullo, R., Jacoby, G. H., & Durrell, P. R. 2003, ApJS, 145, 65
———. 2004a, ApJ, 615, 196
Feldmeier, J. J., Ciardullo, R., Jacoby, G. H., Durrell, P. R., & Mihos, J. C. 2004b, in IAU Symp. 217, Recycling Intergalactic and Interstellar Matter, ed. P.-A. Duc, J. Braine, & E. Brinks (San Francisco: ASP), 64
Ferguson, H. C., Tanvir, N. R., & von Hippel, T. 1998, Nature, 391, 461
Freeman, K. C., et al. 2000, in ASP Conf. Ser. 197, Dynamics of Galaxies: From the Early Universe to the Present, ed. F. Combes, G. A. Mamon, & V. Charmandaris (San Francisco: ASP), 389
Gal-Yam, A., Maoz, D., Guhathakurta, P., & Filippenko, A. V. 2003, AJ, 125, 1087
Gonzalez, A. H., Zabludoff, A. I., Zaritsky, D., & Dalcanton, J. J. 2000, ApJ, 536, 561
Gregg, M. D., & West, M. J. 1998, Nature, 396, 549
Hammer, F., et al. 1997, ApJ, 481, 49

Hogg, D. W., Cohen, J. G., Blandford, R., & Pahre, M. A. 1998, ApJ, 504, 622
Hui, X., Ford, H. C., Ciardullo, R., & Jacoby, G. H. 1993, ApJ, 414, 463
Jacoby, G. H. 1989, ApJ, 339, 39
Jacoby, G. H., Ciardullo, R., & Walker, A. R. 1990, ApJ, 365, 471
Kudritzki, R.-P., et al. 2000, ApJ, 536, 19
Malumuth, E. M., & Richstone, D. O. 1984, ApJ, 276, 413
Marigo, P., Girardi, L., Weiss, A., Groenewegen, M. A. T., & Chiosi, C. 2004, A&A, 423, 995
Méndez, R. H., Kudritzki, R. P., Ciardullo, R., & Jacoby, G. H. 1993, A&A, 275, 534
Merritt, D. 1983, ApJ, 264, 24
———. 1984, ApJ, 276, 26
Miller, G. E. 1983, ApJ, 268, 495
Moore, B., Katz, N., Lake, G., Dressler, A., & Oemler, A. 1996, Nature, 379, 613
Murante, G., et al. 2004, ApJ, 607, L83
Napolitano, N. R., et al. 2003, ApJ, 594, 172
Neilsen, E. H., & Tsvetanov, Z. I. 2000, ApJ, 536, 255
Nulsen, P. E. J., & Bohringer, H. 1995, MNRAS, 274, 1093
Oemler, A. 1973, ApJ, 180, 11
Okamura, S., et al. 2002, PASJ, 54, 883
Peimbert, M. 1990, Rep. Prog. Phys., 53, 1559
Renzini, A., & Buzzoni, A. 1986, in Spectral Energy Distributions of Galaxies, ed. C. Chiosi & A. Renzini (Dordrecht: Reidel), 195
Richstone, D. O., & Malumuth, E. M. 1983, ApJ, 268, 30
Sommer-Larsen, J., Romeo, A. D., & Portinari, L. 2005, MNRAS, 357, 478
Teplitz, H. I., et al. 2000, ApJ, 542, 18
Theuns, T., & Warren, S. J. 1997, MNRAS, 284, L11
Thuan, T. X., & Kormendy, J. 1977, PASP, 89, 466
West, M. J., & Blakeslee, J. P. 2000, ApJ, 543, L27
Willman, B., Governato, F., Wadsley, J., & Quinn, T. 2004, MNRAS, 355, 159
Zibetti, S., White, S. D. M., Schneider, D. M., & Brinkmann, J., 2005, MNRAS, 358, 949
Zwicky, F. 1951, PASP, 63, 61